International Journal of Minerals, Metallurgy and Materials
Volume 22, Number 10, October 2015, Page 1043
DOI: 10.1007/s12613-015-1166-z

Hot deformation mechanism and microstructure evolution of an ultra-high nitrogen austenitic steel containing Nb and V

Rong-hua Zhang[1, 2)], *Ze-an Zhou*[1)], *Ming-wei Guo*[1)], *Jian-jun Qi*[1)], *Shu-hua Sun*[1)], *and Wan-tang Fu*[1)]

1) State Key Laboratory of Metastable Materials Science and Technology, Yanshan University, Qinhuangdao 066004, China

2) College of Metallurgy and Energy, Hebei United University, Tangshan 063009, China

(Received: 2 March 2015; revised: 25 April 2015; accepted: 11 May 2015)

Abstract: The flow curves of an ultra-high nitrogen austenitic steel containing niobium (Nb) and vanadium (V) were obtained by hot compression deformation at temperatures ranging from 1000°C to 1200°C and strain rates ranging from 0.001 s^{-1} to 10 s^{-1}. The mechanical behavior during hot deformation was discussed on the basis of flow curves and hot processing maps. The microstructures were analyzed via scanning electron microscopy and electron backscatter diffraction. The relationship between deformation conditions and grain size after dynamic recrystallization was obtained. The results show that the flow stress and peak strain both increase with decreasing temperature and increasing strain rate. The hot deformation activation energy is approximately 631 kJ/mol, and a hot deformation equation is proposed. (Nb,V)N precipitates with either round, square, or irregular shapes are observed at the grain boundaries and in the matrix after deformation. According to the discussion, the hot working should be processed in the temperature range of 1050°C to 1150°C and in the strain rate range of 0.01 to 1 s^{-1}.

Keywords: austenitic steels; hot deformation; microstructural evolution; nitrides

1. Introduction

High-nitrogen austenitic steels have been widely used in the energy, mechanical, and medical industries because of their good non-magnetic and corrosion resistance and the excellent strength and toughness [1–6]. A typical example of their use is the heavy retaining rings for power generators. However, precipitation usually occurs in the hot working process because of the high alloy content in this type of steel, which leads to the surface cracking during hot forging and deteriorated corrosion resistance during service.

In recent years, researchers have added microalloying elements to improve the properties such as strength and corrosion resistance of high nitrogen stainless steels and studied the deformation mechanism of high nitrogen steel. The addition of vanadium or niobium to ordinary austenitic steels can effectively inhibit the formation of $M_{23}C_6$, thus significantly reducing the intergranular corrosion sensitivity [7]. Knutsen *et al.* [8] indicated that niobium and vanadium could stabilize MX-type precipitates and discontinuous M_2X-type precipitates, respectively. Tarboton *et al.* [9] investigated the effect of chemical composition and deformation temperature on the surface cracking behavior of high nitrogen steel. Their group found that higher Cr content and higher temperature promoted surface cracking. Wang *et al.* [10] studied the influence of $M_{23}C_6$ on the mechanical behavior of high nitrogen steel through hot tensile testing. Their group reported that $M_{23}C_6$ precipitated at the grain boundaries, and its content and precipitation temperature could be reduced by decreasing the C content, which significantly decreased the hot ductility. Kim *et al.* [11] reported that the initial and subsequent deformation processes of high nitrogen steel were controlled by slipping and twinning, respectively. Dislocation and twinning characteristics in high nitrogen steel were studied by Shin and Lee [12]. Their group found that, because of the substructure transformation from dislocation to cross twinning, the strain hardening exponent was improved by increasing the strain from 10% to 50%. However, this transformation decreased

Corresponding author: Wan-tang Fu E-mail: wtfu@ysu.edu.cn

the peak strain. Hong *et al.* [13] found that the dislocation density and twining in high nitrogen steel were the highest at 800°C, and the grain boundary carbides precipitated at this temperature. Furthermore, Lang *et al.* [14] obtained the hot deformation activity energy (764.5 kJ/mol) and the critical strain for recrystallization (0.51) in high nitrogen steel (0.56wt% N) through thermal simulation.

However, the ultra-high nitrogen steel is difficult to deform by hot working because of the high work hardening rate caused by the high N content (≥ 0.9wt%). Furthermore, the precipitation behavior and the influence of vanadium (V) and niobium (Nb) precipitation on the hot deformation in high-alloy steels, especially ultra-high nitrogen steels, are not clear to date.

In the present work, the deformation behavior of ultra-high nitrogen austenitic steel containing Nb and V was analyzed in the temperature range of 1000°C to 1200°C and in the strain rate range of 0.001 to 10 s^{-1}. The hot deformation equation, hot processing maps, and microstructure characteristics were discussed to provide a theoretical basis for establishing the hot working process.

2. Experimental

The tested steel was melted in a pressurized induction furnace, and its chemical composition (wt%) was as follows: 0.11 C, 18.52 Cr, 14.59 Mn, 3.06 Mo, 0.91 N, 0.28 Nb, 0.63 V, 0.69 Si, and balance Fe. The forged ingot was held at 1200°C for 2 h, and then machined into hot compression test specimens with sizes of ϕ8 mm × 12 mm. Hot compression tests were conducted using a Gleeble-3500 thermal/mechanical simulator. The specimens were preheated to 1200°C for 5 min, cooled to the testing temperature at a rate of 10°C·s^{-1}, and then held for 10 s to eliminate the temperature gradient. Tests were performed at temperatures of 1000°C to 1200°C and strain rates of 0.001 to 10 s^{-1}. All samples were deformed to a strain of 0.8 and then instantly quenched with water. For metallographic examination, the deformed specimens were cut along the axis, polished, and etched using a solution of aqua regia (HNO_3:HCl = 1:3 by volume). The microstructures were observed by scanning electron microscopy (SEM) and electron backscatter diffraction (EBSD). Moreover, the average dynamic recrystallization grain size was measured by interception.

3. Results and discussion

3.1. Flow curves

The flow curves of the tested steel at deformation temperatures of 1000°C to 1200°C and strain rates of 0.001 to 10 s^{-1} are shown in Fig. 1. Both flow stress and peak strain increase with decreasing temperature and increasing strain rate. At the same deformation temperature, a higher strain rate corresponds to larger work hardening rate, peak stress, and steady stress. At the same strain rate, the softening rate and content as well as the peak stress and steady stress increase with increasing temperature. For each flow curve in Fig. 1, the flow stress decreases with increasing strain when the flow stress reaches a peak. A platform appears when the strain rate is lower than 0.01 s^{-1} and the temperature is higher than 1050°C, which is typical of fully dynamic recrystallization [15].

3.2. Hot deformation equation

In the thermal deformation of metal materials, the flow stress is related to chemical composition, temperature (T), deformation (ε), and strain rate ($\dot{\varepsilon}$). When the chemical composition is determined, the relationship between flow stress (σ) and deformation conditions can be described by the classical hyperbolic sine function, as shown in Eq. (1) [16].

$$\dot{\varepsilon} = A[\sinh(\alpha \cdot \sigma)]^n \exp(-Q/RT) \quad (1)$$

where A and α are the material constants that are independent of deformation temperature, σ the steady flow stress, n the stress exponent, Q the hot deformation activation energy, R the gas constant, and T the absolute temperature. In this study, σ was taken as the peak stress.

The relation curve between peak stress and temperature can be obtained after processing the flow curve in Fig. 1. Through the linear regression, the following average values of every parameter were obtained as $A = 3.34\times10^{22}$, $\alpha = 0.00573$, $n = 4.79$, and $Q = 631$ kJ/mol. High alloy content and precipitates lead to a higher hot deformation activation energy. The hot deformation equation of the tested steel can be expressed as

$$\dot{\varepsilon} = 3.34\times10^{22}[\sinh(0.00573\sigma)]^{4.79} \exp(-631000/RT). \quad (2)$$

3.3. Microstructure

The initial microstructure of ultra-high nitrogen austenitic steel containing Nb and V is a single-phase austenite with a grain size of 74 μm. Fig. 2 shows the electron backscatter diffraction (EBSD) and misorientation angle maps of specimens deformed at different deformation conditions. Fig. 2(a) shows that the parent grains are elongated and surrounded by newly formed dynamic recrystallization (DRX) grains (i.e., necklace structure). Fig. 2(b) shows that the number

number fractions of high-angle (≥ 15°) and low-angle (< 15°) grain boundaries are similar in the specimen deformed at 1000°C. At 1100°C in Fig. 2(c), both the DRX content and grain size are larger than those in Fig. 2(a). Fig. 2(d) shows that low-angle grain boundaries are still observed with a number fraction of approximately 0.25. When the deformation temperature reaches 1200°C, the DRX grain size is approximately 20 μm, and no elongated grains exist. The corresponding misorientation angle map reveals a completed DRX structure in Fig. 2(f).

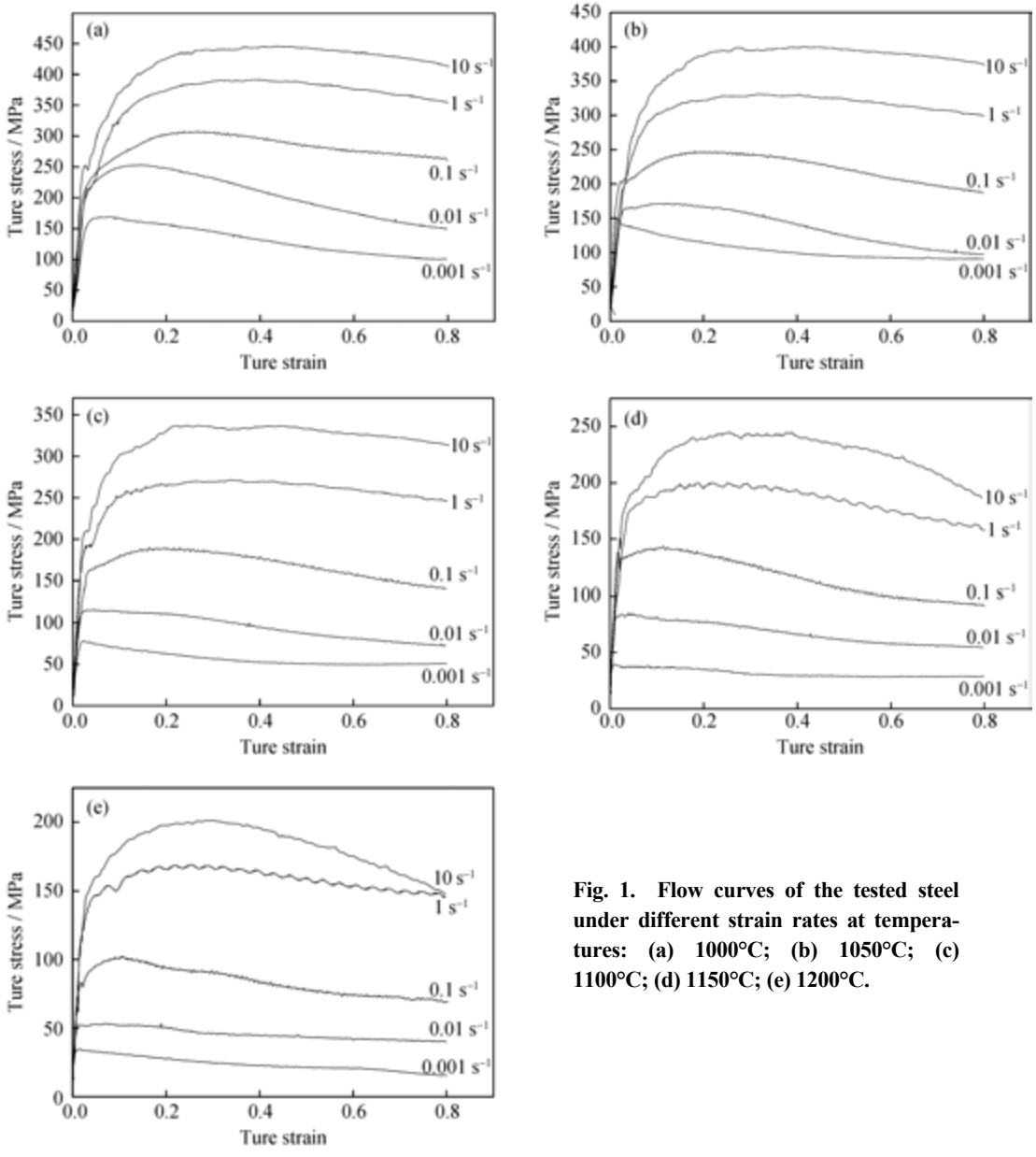

Fig. 1. Flow curves of the tested steel under different strain rates at temperatures: (a) 1000°C; (b) 1050°C; (c) 1100°C; (d) 1150°C; (e) 1200°C.

The DRX grain sizes are measured via the line intercept, and their dependence on deformation conditions is shown in Fig. 3. After fitting, the quantitative relationship can be obtained, as shown in Eq. (3)

$$D = 9.05 \times (Z/A)^{-0.087} \quad (3)$$

where D stands for the dynamic recrystallization grain size, Z the Zener–Hollomon parameter, and A the material constant.

3.4. Processing maps

The theoretical basis and methods for establishing hot processing maps have been previously described in detail by Prasad [17]. A work piece deformed at hot working conditions can be considered to be a power dissipater. The strain rate sensitivity index (m) for determining the distribution of system power dissipation caused by viscous-plastic deformation

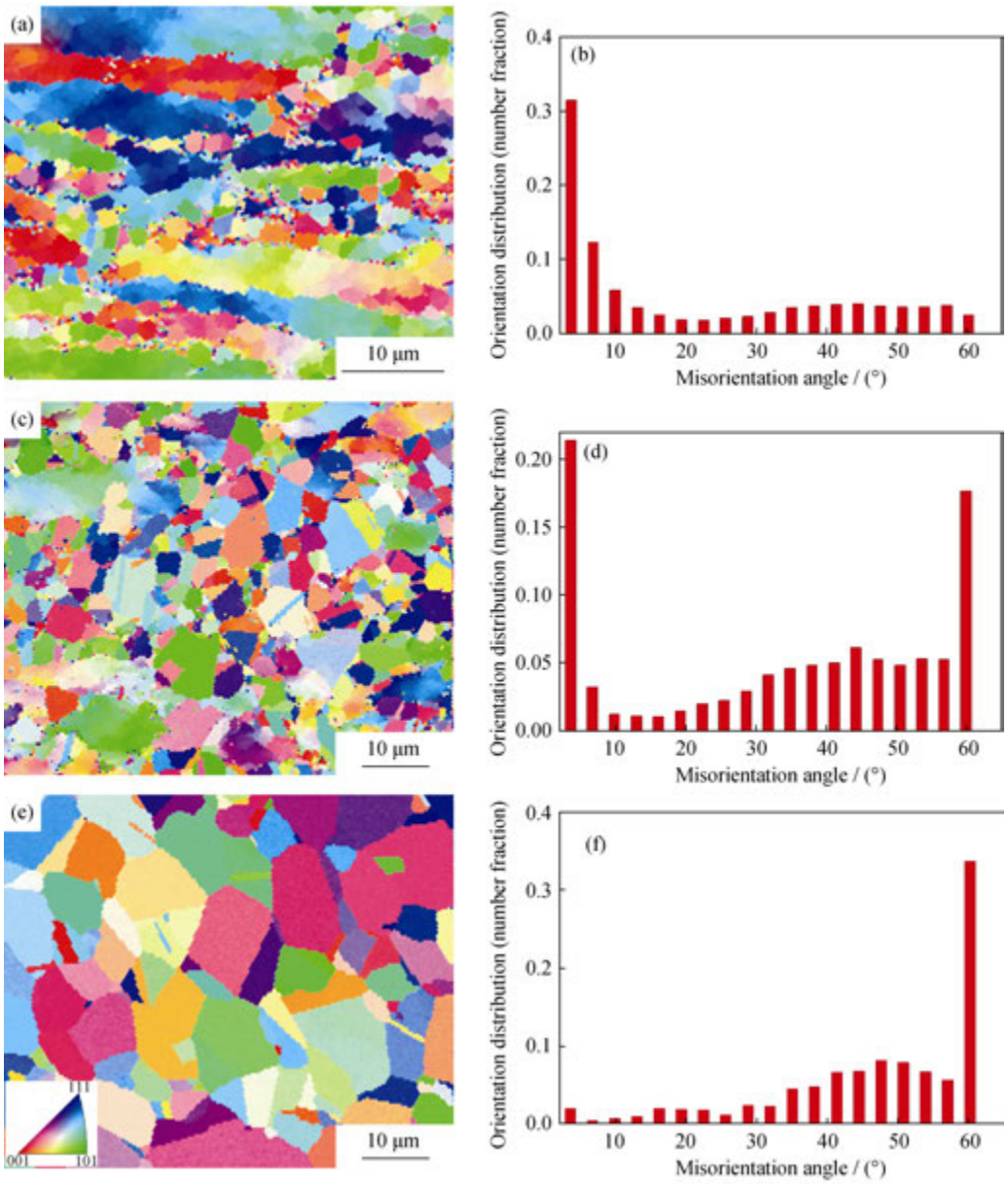

Fig. 2. EBSD and misorientation angle maps of specimens deformed at different deformation conditions (true strain 0.8): (a) and (b) 1000°C, 1 s^{-1}; (c) and (d) 1100°C, 1 s^{-1}; (e) and (f)1200°C, 1 s^{-1}

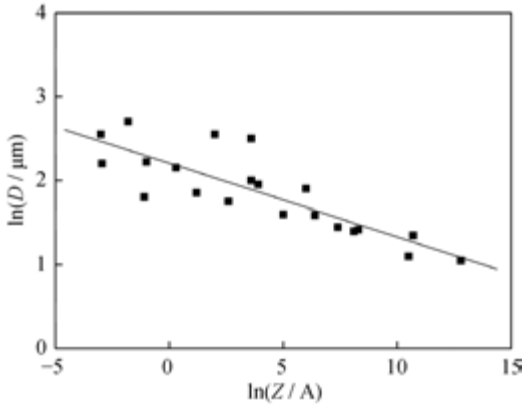

Fig. 3. Relationship between deformation condition and DRX grain size.

because of structural changes is denoted by the power dissipation ratio (η) due to the structural changes in the deformation process, which is indicated how efficiently the material dissipates energy under microstructural changes. This finding can be defined by Eq. (4).

$$\eta = \frac{2m}{m+1} \tag{4}$$

where η is the energy change in the microstructure, which varies with deformation temperature and strain rate, and m is the strain sensitivity index of flow stress and can be given by Eq. (5).

$$m = \frac{\Delta \ln \sigma}{\Delta \ln \dot{\varepsilon}} \tag{5}$$

The power dissipation map can be obtained based on the values of η under different conditions. Eq. (6) shows the flow instability criteria (ξ).

$$\xi = \frac{\partial \ln[m/(m+1)]}{\partial \ln \dot{\varepsilon}} + m < 0 \tag{6}$$

Flow instabilities are expected when ξ is negative. The instability map can be superimposed on the power dissipation map to obtain a processing map.

The hot processing map of ultra-high nitrogen austenitic steel containing Nb and V is shown in Fig. 4, where the values of isoclines represent the percentage of power dissipation at that condition, and the shadow area represents flow instability. As observed, the power dissipation (η) increases with increasing temperature and decreasing strain rate. The percentage of energy dissipation rate reaches a maximum of 65% at 1200°C and 0.001 s^{-1} at a strain of 0.8 in Fig. 4(d). Moreover, the flow instability mostly appears in the high strain rate area (1 to 10 s^{-1}). The temperature range of flow instability varies with deformation amount. The area of instability at temperatures ranging from 1000°C to 1200°C is larger at strains of 0.2 and 0.4, and it significantly decreases with increasing strain. Thus, the suggested processing window is 1050°C–1150°C and 0.01–1 s^{-1}.

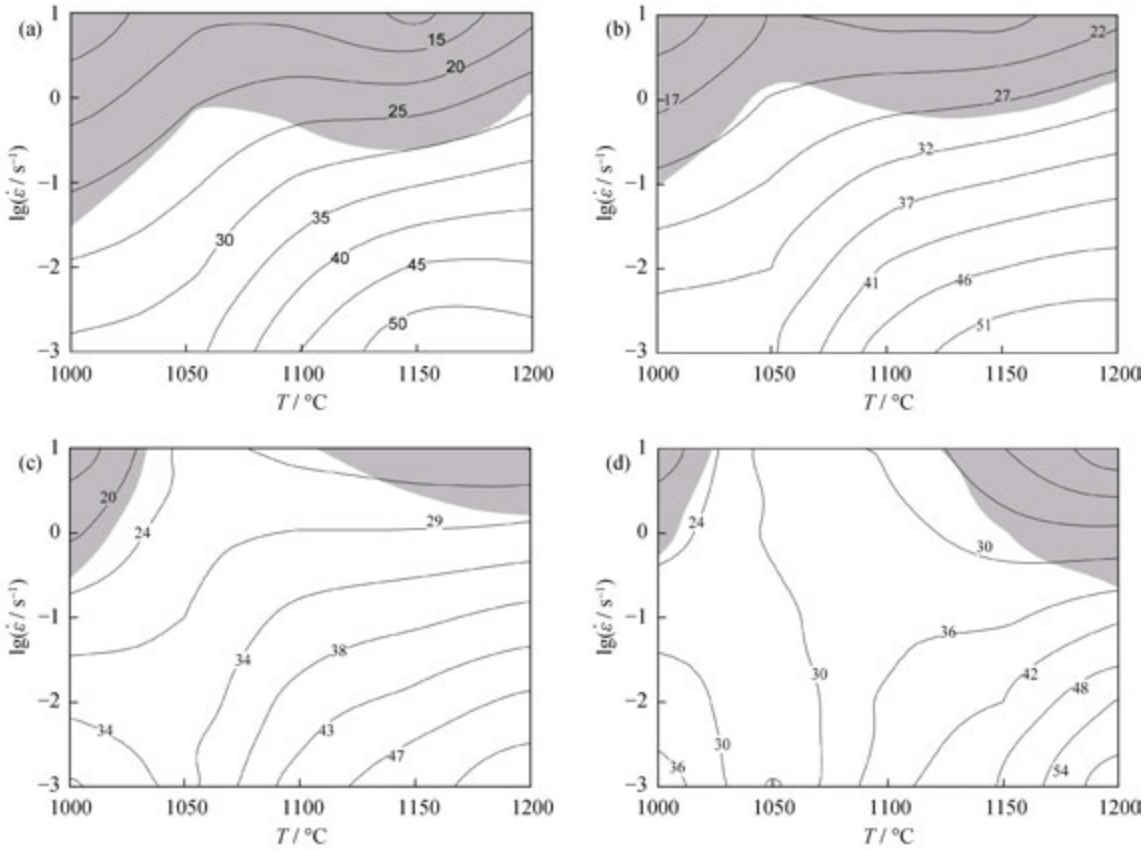

Fig. 4. Hot processing maps obtained on the tested steel at different strains: (a) 0.2; (b) 0.4; (c) 0.6; (d) 0.8

3.5. Precipitate phase

According to the Ref. [18], the second phase would precipitate at the grain boundary or dislocate in the hot deformation process in austenitic steel (0.36wt% N, 0.29wt% Nb). The sizes of particles were different; the plate-like particles were as large as 15 μm, the round particles were 1 μm to 2 μm, and the smallest particles were approximately 0.3 μm.

The morphology and composition of the precipitate at 1150°C and 1.0 s^{-1} are shown in Fig. 5. Apparently, many small particles are at the grain boundaries and in the matrix. The intragranular precipitate phase is round ellipse or irregular in shape with a size of ~220 nm, and the intergranular precipitates are square or irregular with sizes of ~580 nm. These precipitates can pin grain boundaries and refine grain size during hot deformation. Energy-dispersive X-ray spectroscopy (EDS) analysis of precipitate in Fig. 5(b) shows that the particle is MX type, i.e., (Nb,V)N. NbN and VN are completely miscible because of their same face-centered cubic structure and similar lattice constant. The precipitate

particles grow following the Ostwald ripening mechanism. The effect of precipitation strengthening is further enhanced with increasing the number of small-sized particles and decreasing temperature.

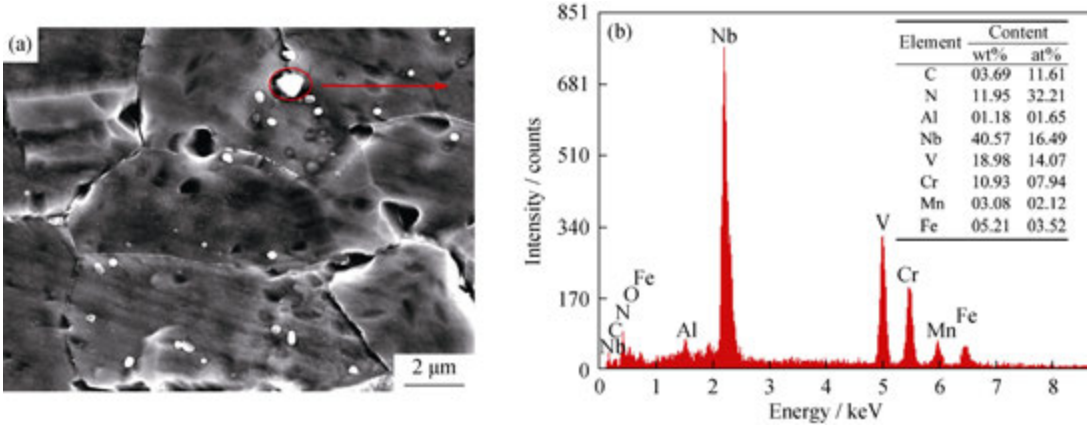

Fig. 5. Scanning electron microscopy image (a) and EDS spectrum (b) of precipitates in the tested steel at 1150°C and 1.0 s^{-1}.

4. Conclusions

(1) The flow curves of ultra-high nitrogen austenitic steel are obtained at temperatures ranging from 1000°C to 1200°C and strain rates ranging from 0.001 to 10 s^{-1}. The peak stress and flow stress both increase with decreasing deformation temperature and increasing strain rate.

(2) The hot deformation activation energy at temperatures of 1000°C to 1200°C and strain rates of 0.001 to 10 s^{-1} is 631 kJ/mol.

(3) The hot processing maps of ultra-high nitrogen austenitic steel containing Nb and V are obtained. The power dissipation (η) increases with increasing temperature and decreasing strain rate. Moreover, the suggested processing window is 1050°C–1150°C and 0.01–1 s^{-1}.

(4) Many small particles (Nb,V)N are located at grain boundaries and in the deformed matrix of the ultra-high nitrogen austenitic steel. The intragranular precipitate phase is round, ellipsoidal, or irregular with a size of ~220 nm, and the intergranular precipitates are square or irregular with sizes of ~58 nm.

Acknowledgements

This work was financially supported by the Natural Science Foundation–Steel and Iron Foundation of Hebei Province (No. E2013203110) and the Foundation for Young Scholars in Yanshan University (No. 14LGA004).

References

[1] J.M. Simmons, Overview: high-nitrogen alloying of stainless steels, *Mater. Sci. Eng. A*, 207(1996), No. 2, p. 159.

[2] M.O. Speidel, Nitrogen containing austenitic stainless steels, *Mater. Sci. Eng. Technol.*, 37(2006), No. 10, p. 875.

[3] W.T. Fu, Y.Z. Zheng, and X.K. He, Resistance of a high nitrogen austenitic steel to cavitation erosion, *Wear*, 249(2001), No. 9, p. 788.

[4] A. Di Schino, J.M. Kenny, M.G. Mecozzi, and M. Barteri, Development of high nitrogen, low nickel, 18%Cr austenitic stainless steels, *J. Mater. Sci.*, 35(2000), No. 19, p. 4803.

[5] Z.H. Jiang, Z.R. Zhang, H.B. Li, Z. Li, and Q.F. Ma, Microstructural evolution and mechanical properties of aging high nitrogen austenitic stainless steels, *Int. J. Miner. Metall. Mater.*, 17(2010), No. 6, p. 729.

[6] H.B. Li, Z.H. Jiang, Y. Yang, Y. Cao, and Z.R. Zhang, Pitting corrosion and crevice corrosion behaviors of high nitrogen austenitic stainless steels, *Int. J. Miner. Metall. Mater.*, 16(2009), No. 5, p. 517.

[7] A.F. Padilha, I.F. Machado, and R.L. Plaut, Microstructures and mechanical properties of Fe–15%Cr–15%Ni austenitic stainless steels containing different levels of niobium additions submitted to various processing stages, *J. Mater. Process. Technol.*, 170(2005), No. 1-2, p. 89.

[8] R.D. Knutsen, C.I. Lang, and J.A. Basson, Discontinuous cellular precipitation in a Cr–Mn–N steel with niobium and vanadium additions, *Acta Mater.*, 52(2004), No. 8, p. 2407.

[9] J.N. Tarboton, L.M. Matthews, A. Sutcliffe, C.M.P. Frost, and J.P. Wessels, The hot workability of Cromanite™, a high nitrogen austenitic stainless steel, *Mater. Sci. Forum*, 318-320(1999), p. 777.

[10] L.J. Wang, L.Y. Sheng, and C.M. Hong, Influence of grain boundary carbides on mechanical properties of high nitrogen austenitic stainless steel, *Mater. Des.*, 37(2012), p. 349.

[11] Y.S. Kim, S.M. Nam, and S.J. Kim, Strain rate dependence of deformation behavior of high-nitrogen austenitic steels, *J. Mater. Process. Technol.*, 187-188(2007), p. 575.

[12] J.H. Shin and J.W. Lee, Effects of twin intersection on the tensile behavior in high nitrogen austenitic stainless steel,

Mater. Charact., 91(2014), p. 19.

[13] C.M. Hong, J. Shi, L.Y. Sheng, W.C. Cao, W.J. Hui, and H. Dong, Effects of hot-working parameters on microstructural evolution of high nitrogen austenitic stainless steel, *Mater. Des.*, 32(2011), No. 7, p. 3711.

[14] Y.P. Lang, Y. Zhou, F. Rong, H.T. Chen, Y.Q. Weng, and J. Su, Hot working of high nitrogen austenitic stainless steel, *J. Iron Steel Res. Int.*, 17(2010), No. 10, p. 45.

[15] M. Haj, H. Mansouri, R. Vafaei, G.R. Ebrahimi, and A. Kanani, Hot compression deformation behavior of AISI 321 austenitic stainless steel, *Int. J. Miner. Metall. Mater.*, 20(2013), No. 6, p. 529.

[16] W.H. Zhang, S.H. Sun, D.L. Zhao, B.Z. Wang, Z.H. Wang, and W.T. Fu, Hot deformation behavior of a Nb-containing 316LN stainless steel, *Mater. Des.*, 32(2011), No. 8-9, p. 4173.

[17] Y.V.R.K. Prasad and S. Sasidhara, *Hot Working Guide*: *A Compendium of Processing Maps*, ASM International, 1997, p. 3.

[18] E.S. Silva, R.C. Sousa, A.M. Jorge, and O. Balancin, Hot deformation behavior of an Nb- and N-bearing austenitic stainless steel biomaterial, *Mater. Sci. Eng. A*, 543(2012), p. 69.